

Current-induced skyrmion generation through morphological thermal transitions in chiral ferromagnetic heterostructures

Ivan Lemesh, Kai Litzius, Marie Böttcher, Pedram Bassirian, Nico Kerber, Daniel Heinze, Jakub Zázvorka, Felix Büttner, Lucas Caretta, Maxwell Mann, Markus Weigand, Simone Finizio, Jörg Raabe, Mi-Young Im, Hermann Stoll, Gisela Schütz, Bertrand Dupé, Mathias Kläui, Geoffrey S. D. Beach

Angaben zur Veröffentlichung / Publication details:

Lemesh, Ivan, Kai Litzius, Marie Böttcher, Pedram Bassirian, Nico Kerber, Daniel Heinze, Jakub Zázvorka, et al. 2018. "Current-induced skyrmion generation through morphological thermal transitions in chiral ferromagnetic heterostructures." *Advanced Materials* 30 (49): 1805461.
<https://doi.org/10.1002/adma.201805461>.

Nutzungsbedingungen / Terms of use:

licgercopyright

Dieses Dokument wird unter folgenden Bedingungen zur Verfügung gestellt: / This document is made available under the following conditions:

Deutsches Urheberrecht

Weitere Informationen finden Sie unter: / For more information see:

<https://www.uni-augsburg.de/de/organisation/bibliothek/publizieren-zitieren-archivieren/publizieren>



Current-Induced Skyrmion Generation through Morphological Thermal Transitions in Chiral Ferromagnetic Heterostructures

Ivan Lemes, Kai Litzius, Marie Böttcher, Pedram Bassirian, Nico Kerber, Daniel Heinze, Jakub Zázvorka, Felix Büttner, Lucas Caretta, Maxwell Mann, Markus Weigand, Simone Finizio, Jörg Raabe, Mi-Young Im, Hermann Stoll, Gisela Schütz, Bertrand Dupé, Mathias Kläui, and Geoffrey S. D. Beach**

Magnetic skyrmions promise breakthroughs in future memory and computing devices due to their inherent stability and small size. Their creation and current driven motion have been recently observed at room temperature, but the key mechanisms of their formation are not yet well-understood. Here it is shown that in heavy metal/ferromagnet heterostructures, pulsed currents can drive morphological transitions between labyrinth-like, stripe-like, and skyrmionic states. Using high-resolution X-ray microscopy, the spin texture evolution with temperature and magnetic field is imaged and it is demonstrated that with transient Joule heating, topological charges can be injected into the system, driving it across the stripe-skyrmion boundary. The observations are explained through atomistic spin dynamic and micromagnetic simulations that reveal a crossover to a global skyrmionic ground state above a threshold magnetic field, which is found to decrease with increasing temperature. It is demonstrated how by tuning the phase stability, one can reliably generate skyrmions by short current pulses and stabilize them at zero field, providing new means to create and manipulate spin textures in engineered chiral ferromagnets.

Magnetic skyrmions represent a class of topological chiral spin textures that can be found in bulk materials^[1–3] as well as in thin magnetic films and multilayers^[4–7] with perpendicular magnetic

anisotropy (PMA). In ultrathin films, skyrmions can exhibit sub-nanometer scale size^[8–11] and move in response to an applied current with velocities exceeding 100 m s^{-1} ^[5] in a controllable^[12,13] and reliable^[13] way. Therefore, they promise great technological utility for racetrack-type memories,^[14] logic gates,^[15] probabilistic computing,^[16] and neuromorphic devices,^[17] for which they have to be readily created and manipulated. Homochiral skyrmions can be stabilized by the Dzyaloshinskii–Moriya interaction (DMI)^[18,19] in materials with strong spin-orbit coupling and broken inversion symmetry. Since asymmetric multilayer stacks of a ferromagnet and a heavy metal^[5–7] possess DMI and can also exhibit large current-induced spin-orbit torques that can provide an efficient means to create and manipulate skyrmions,^[20–22] these systems are now a central focus of current research.

Magnetic skyrmions can exist as isolated topological excitations,^[23,24] or as ordered arrays (hexagonal lattice) comprising the magnetic ground state,^[2,5] depending on material and

I. Lemes, Dr. F. Büttner, L. Caretta, Dr. M. Mann, Prof. G. S. D. Beach
Department of Materials Science and Engineering
Massachusetts Institute of Technology
Cambridge, MA 02139, USA
E-mail: gbeach@mit.edu

K. Litzius, M. Böttcher, P. Bassirian, N. Kerber, D. Heinze,
Dr. J. Zázvorka, Dr. B. Dupé, Prof. M. Kläui
Institute of Physics
Johannes Gutenberg-University Mainz
55099 Mainz, Germany
E-mail: klaeui@uni-mainz.de

K. Litzius, Prof. M. Kläui
Graduate School of Excellence Materials Science in Mainz
55128 Mainz, Germany

K. Litzius, Dr. M. Weigand, Dr. H. Stoll, Prof. G. Schütz
Max Planck Institute for Intelligent Systems
70569 Stuttgart, Germany

Dr. S. Finizio, Dr. J. Raabe
Swiss Light Source
Paul Scherrer Institut
Villigen PSI CH-5232, Switzerland

Dr. M.-Y. Im
Center for X-ray Optics
Lawrence Berkeley National Laboratory
Berkeley, CA 94720, USA

Dr. M.-Y. Im
Department of Emerging Materials Science
DGIST
Daegu 42988, Republic of Korea

Dr. M.-Y. Im
School of Materials Science and Engineering
Ulsan National Institute of Science and Technology (UNIST)
Ulsan 44919, Republic of Korea

 The ORCID identification number(s) for the author(s) of this article can be found under <https://doi.org/10.1002/adma.201805461>.

DOI: 10.1002/adma.201805461

environmental parameters. The skyrmion lattice state^[25] in bulk materials resides in a well-defined pocket of field-temperature phase space, separated from other morphologies such as the spin-spiral and uniform ferromagnetic states. Transitions among these states have been well-characterized in bulk B20-compounds^[26] and in symmetric Fe/Gd ferrimagnetic multilayers,^[27] but less so in applications-relevant ferromagnet/heavy-metal heterostructures.^[5] In such materials, skyrmion creation has been demonstrated using inhomogeneous in-plane currents in planar structures with patterned constrictions,^[28,29] at defects due to the action of current-induced spin-transfer or spin-orbit torques^[22,30–33] and with homogeneous current if a skyrmion nucleation center is already present.^[34] However, these mechanisms rely on extrinsic effects and the existing studies provide little insight into the energetics and thermal stability of skyrmions with respect to other magnetic states. Moreover, although the large current densities involved in heavy-metal/ferromagnet multilayers often result in significant Joule heating that can directly affect the nucleation of magnetic skyrmions,^[21,22] most recent studies have either completely ignored the role of temperature in skyrmion formation or considered it trivially, focusing only on the temperature dependence of the magnetic properties of the system. The underlying physical processes of such thermally induced nucleation still remain unclear.

A recent theoretical study has revealed through atomistic simulations that thermal energy alone can lead to dynamical changes in the net skyrmion charge Q in Pd/Fe/Ir(111) ultrathin films.^[35] Here, we experimentally find a similar thermally driven increase in Q after injecting current pulses into Pt/CoFeB/MgO multilayers with ultralow-pinning. We study the current-induced magnetic patterns as a function of magnetic field and temperature and show that current pulses can be used to drive transitions amongst skyrmionic, labyrinth, and stripe-like morphologies in a controllable way. We find that the resulting magnetic pattern is defined mainly by the peak transient sample temperature during the pulse transmission, while current-induced torques play a minor role. By using atomistic Langevin spin dynamics simulations, we demonstrate directly how the skyrmion generation occurs through thermal excitations of the initial stripe state. This work yields key insights into the generation of various morphological states in chiral ferromagnets, their relative stability, and the thermally driven transformations between them. Our findings have practical applications, including the creation, stability, and current-driven motion of zero-field skyrmions, and reliable skyrmion generation using single current pulses with a duration down to a few ns.

For this study, we have synthesized thin films of [Pt(2.7 nm)/CoFeB(0.86 nm)/MgO(1.5 nm)]_{x15} multilayers grown by sputter deposition and patterned into two-micrometer wide tracks with contacts at either end for electrical current pulse injection (see the Experimental Section). The resulting material (Figure 1a) exhibits PMA with an in-plane saturation field of 0.9 T and the out-of-plane hysteresis loop shown in Figure 1b, where the low zero-field remanence implies a multidomain state. The DMI constant is $D \approx 1.76 \text{ mJ m}^{-2}$, which is sufficient to ensure a homochiral Néel texture for domain walls and skyrmions,^[36] as calculated in the Supporting Information and evidenced experimentally below. For this material, we

employ high-resolution scanning transmission X-ray microscopy (STXM) (Figure 1c) to perform temperature-dependent imaging of magnetic states.

First, we reveal the distinct room temperature magnetic states that the system exhibits, which can be accessed through current-pulse excitation under various magnetic bias fields. Prior to all measurements we apply an alternating-field demagnetization cycle, which yields an initial multidomain state with a labyrinth character as depicted in Figure 1d. This state develops from some random elements of the demagnetization cycle (the field inhomogeneities, geometry and original magnetization pattern) and does not necessarily correspond to a global energy minimum.^[37,38] The effects of the application of a train of 10^4 bipolar current pulses with the voltage of 2.6 V and pulse width of 7.5 ns (corresponding to a current density $j \approx 4.3 \times 10^{11} \text{ A m}^{-2}$) are shown in Figure 1e–g for increasing values of the out-of-plane (OOP) magnetic field at room temperature. Here, bipolar pulses are used instead of unipolar pulses to minimize current-induced displacement and thus highlight changes to the magnetic state. At zero field, the labyrinth structure evolves into a system of aligned stripes, as can be seen in Figure 1e. The stripes can align either parallel or orthogonal to the current flow depending on the applied voltage (see the Supporting Information). Under absence of a magnetic field, no further evolution of orthogonal stripes state occurs upon subsequent current-pulse injection. However, if the same pulse excitation is applied in conjunction with an OOP bias field, skyrmions are produced (Figure 1f,g), either coexisting with stripes at lower field (Figure 1f) or as a disordered array at higher field (Figure 1g). We find that skyrmions are generated regardless of the initial state as long as the current density is above some threshold value $J_{\text{thr}}^{\text{sky}}$ (which is dependent on magnetic field and temperature) and the field is below the saturation value.

Figure 1h,i shows that the effects of current pulses are cumulative, and that with fewer pulses injected (here 100 pulses, with similar characteristics as in Figure 1e–g), the transition to the skyrmionic state is incomplete.

The state in Figure 1i allows us to conveniently probe the effects of current-induced spin-orbit torques on domains and skyrmions simultaneously, and to verify their homochiral nature and low-pinning behavior. We find a critical current for domain wall and skyrmion displacement of $\approx 1 \times 10^{11} \text{ A m}^{-2}$ in this material, consistent with previous experiments.^[5,13] As seen in Figure 1j,k, single unipolar current pulses act to uniformly displace both the stripe domains and the skyrmions, in a direction opposite to the electron flow, consistent with the expected behavior for left-handed chiral Néel domain walls and skyrmions under the action of the damping-like torque induced by spin accumulation due to the spin Hall effect in Pt.^[39,40] The concurrent and synchronous displacement of all magnetic features indicates an absence of strong pinning centers in this material, as also evidenced in pump-probe experiments (see Movie in the Supporting Information) and in our earlier work.^[13] Hence, the current-induced skyrmion generation that we examine here is fundamentally different from that studied in prior works,^[22,30–34] where local inhomogeneities such as pinning centers mediated the skyrmion nucleation.

Next, we focus on understanding the conditions leading to pulsed-current skyrmion generation. For this, we fix the applied

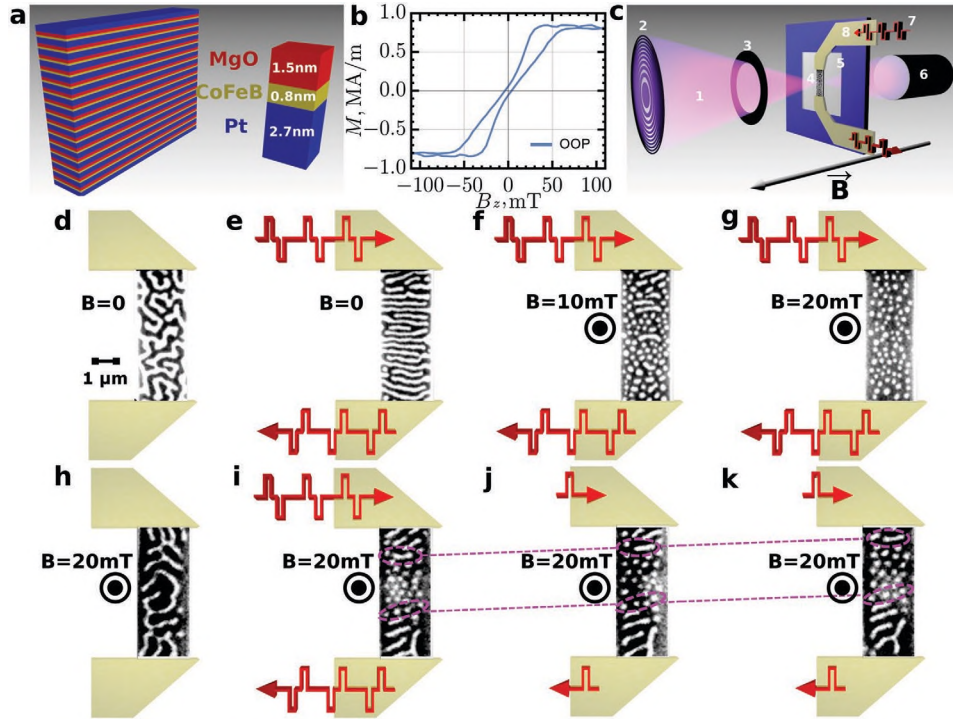


Figure 1. Experimental setup and the effect of the applied field and current pulse excitation. a) Schematic multilayer stack of Pt/CoFeB/MgO with 15 repeats and b) measured out-of-plane hysteresis loop. c) Experimental schematic of the setup used for scanning transmission X-ray microscopy (STXM) experiments: An X-ray beam (1) is focused with a zone plate (2) on the sample (4) located on a SiN membrane (5) in the presence of an applied out-of-plane magnetic field. An order selecting aperture (3) is employed to pass the first order diffraction and to avoid the illumination of the sample from the zero-order light. The transmitted beam is collected at the detector (6). The current pulses (7) are injected through gold pads (8) that are connected to the sample. d–g) Magnetic states resulting from the application of trains of 10 000 bipolar pulses with 7.5 ns pulse width and (transmitted) pulse amplitude $U = 2.6$ V to d) the initial demagnetized state leading to e) the aligned stripe state, f) the mixed state, and g) the skyrmion state. Another mixed state (i) has been achieved by applying a train of 100 pulses with $U = 2.7$ V and 5 ns pulse width from the initial labyrinth state at 20 mT (h). j, k) The subsequent homogeneous motion has been induced by the repeated application of single unipolar pulses with $U = 3.6$ V and 5 ns pulse width.

OOP magnetic field to the values at which a skyrmion lattice can be easily accessed, and vary the current pulse characteristics. **Figure 2a** depicts the result of applying bipolar pulse trains as a function of pulse amplitude at 40 mT. One can observe a sharp transition to the skyrmion state at the pulse voltage of $U_{\text{thr}}^{\text{sky}} \approx 1.8$ V (corresponding to $j_{\text{thr}}^{\text{sky}} \approx 3.0 \times 10^{11}$ A m $^{-2}$), with no variation of the morphology for larger voltages. If the applied voltage is such that $j < j_{\text{thr}}^{\text{sky}}$, the domains readjust their position, but the intrinsic morphology of the labyrinth/stripe state remains the same.

Since current can apply both a torque (due to spin-orbit effective fields) and energy (due to Joule heating), we vary next the pulse shape characteristics to isolate each of these factors and determine the dominant driver of the morphological transition. **Figure 2b** shows the results of experiments in which we decrease the voltage amplitude of the bipolar pulse trains, but increase the pulse width to maintain identical Joule dissipation. The amplitude of the shortest-duration pulses is chosen to be safely above the threshold

identified in **Figure 2a**. We find that all the resulting states are equivalent, regardless of current pulse amplitude, even when

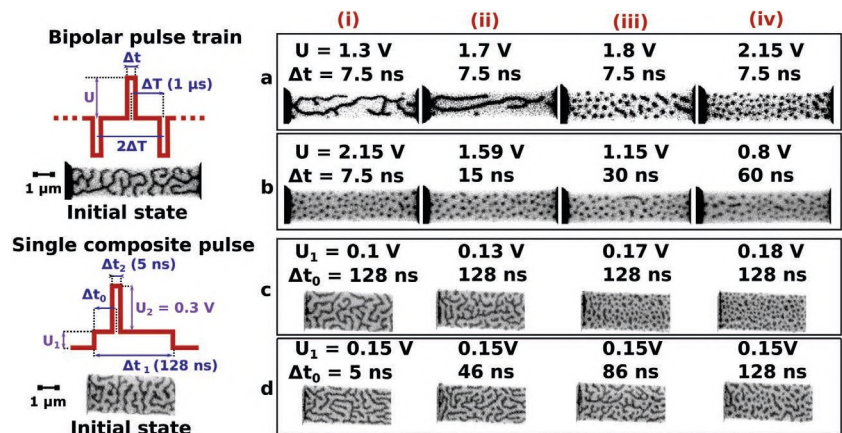


Figure 2. Skyrmion lattice transition for pulses of different amplitude and width. The evolution of the initial labyrinth structure. a, b) By exciting with 10 000 bipolar pulses at 40 mT OOP field: a) as a function of the transmitted voltage of the bipolar pulses with a fixed pulse width of 7.5 ns and b) as a function of the voltage and pulse width, chosen to maintain constant Joule dissipation. c, d) By exciting with a single composite pulse at 15 mT OOP field: c) as a function of the base pulse voltage U_1 at a fixed 128 ns delay of a secondary 5 ns pulse $U_2 = 0.3$ V and d) as a function of the delay Δt_0 of the secondary pulse U_2 . Each subsequent measurement is taken after a short demagnetizing procedure in order to reset the state (denoted as the initial state).

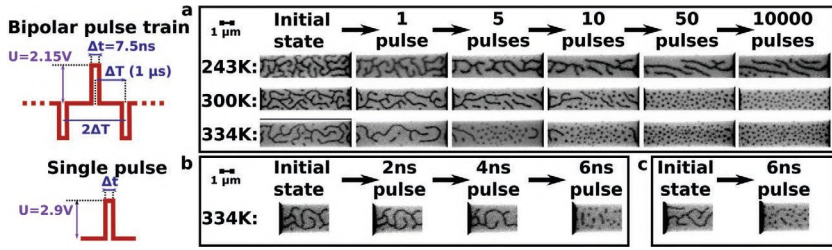


Figure 3. Skyrmion generation as a function of substrate temperature and the number of applied pulses. The evolution of the initial labyrinth state at 40 mT: a) As a function of temperature for sequences of images acquired after increasing numbers of bipolar pulses of $U = 2.15$ V and the individual pulse duration of 7.5 ns. b,c) As a function of the width of a unipolar single pulse of 2.9 V amplitude. Sequence (c) depicts a direct single pulse transition to the skyrmion lattice state.

the amplitude is less than half of the ≈ 1.8 V threshold suggested by Figure 2a (compare panels a(ii) and b(iv)). Since a transformation induced by torques should occur on dynamical time-scales of order 1 ns, and since the experiments in Figure 2b are all isothermal by design, this result indicates that the threshold current for skyrmion generation is not related to the torque-induced nucleation threshold that was previously identified in zero K simulations,^[31,32] but merely a thermal effect. To further highlight this, Figure 2d shows the sequence of measurements in which we apply various single composite pulses that deliver the identical amount of current-induced torque. The pulses consist of a single 5 ns spike of 0.3 V on top of a 128 ns base pulse, with the base amplitude chosen to be near the skyrmion creation threshold of ≈ 0.15 V (see sequence in Figure 2c). By varying the delay Δt_0 of the spike (Figure 2d), we can observe that the final morphologies can be either the labyrinth state (for short delays), or the skyrmion state (for longer delays). Indeed, the longer a delay, the higher the maximum sample temperature, which, as we will see later, can lead to different final states. Thus, the results observed in Figure 2b,d confirm that the transition to a skyrmionic state is thermally induced, in accordance with a similar suggestion made in ref. [21].

To directly ascertain the importance of temperature, we perform experiments at varying substrate temperatures, using a temperature-controlled cryostat. We begin by applying an increasing number of bipolar pulse trains of fixed amplitude and at constant magnetic field as presented in Figure 3a. We observe that for these pulse parameters, single pulses are insufficient to generate skyrmions, but as the number of pulses increases, skyrmion generation is eventually observed. A key observation is that the number of pulses required depends strongly on the nominal substrate temperature. At 334 K it only takes a few pulses to trigger the skyrmion transition, while at 243 K, even the application of 10 000 pulses generates only a few skyrmions. These results suggest that there is a critical temperature at which the skyrmion transition occurs, and that the energy of a single pulse does not heat the sample enough at these substrate temperatures, but cumulative heating by multiple pulses sufficiently raises the sample temperature.

Our in situ real-time resistance measurements (see the Supporting Information) indicate that the fabricated wires heat up by ≈ 100 K at the peak of the pulse injection, which results in noticeable STXM contrast variations during dynamic

pump-probe measurements (see Movie in the Supporting Information). This heating also allows us to understand the observation in Figure 1i wherein the partial generation of skyrmions occurs away from the contact pads. The pads act as heat sinks, so the temperature near the middle of the wire is higher than at its ends where stripes remain.^[41]

One can anticipate then that single, short current pulses should generate skyrmions if the amplitude is large enough to heat the sample beyond the skyrmion transition temperature. This is demonstrated in Figure 3b, in which we apply a single unipolar pulse of fixed 2.9 V amplitude with increasing pulse width, and find that a 6 ns long pulse completely transforms the system to a skyrmionic state.

To understand the origin of the observed morphological transitions, we now examine the zero K energetics of the labyrinth, stripe, and skyrmion patterns versus the OOP magnetic field, which we find in Figure 1e–g to be critical in determining the final state after current-pulse excitation. For each pattern and field, we employed micromagnetic simulations (see the Experimental Section) and identified the states with minimum total energy, which we depict in Figure 4. First, we see that the ground state of the system transitions from the ordered stripe phase to the skyrmions lattice phase as the OOP field crosses a threshold B_{thr} (30 mT in Figure 4). We can also see that the labyrinth state, with which we initialize all our experiments, is always the highest in energy, no matter what field is applied. This state, however, can still represent a local energy minimum,^[38] as transitioning to a ground state requires overcoming energy barriers associated with the creation of intermediate high-energy states.^[37]

To check if heating the system (via either current-induced Joule heating or sample heating) can help overcome such barriers and access transitions between the different states, we employ atomistic spin dynamics simulations at finite temperature (see the Experimental Section). The results are presented in Figures 5a,b. We first have run simulations for three normalized

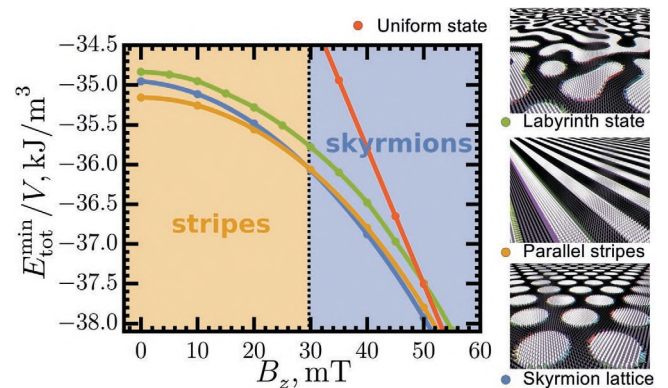


Figure 4. Micromagnetic simulations of the energetics of Néel skyrmion lattice, periodic parallel stripe domains, and labyrinth domains at 0 K. Simulated spin textures equilibrated with respect to the domain spacing, the domain size, and the domain wall width (see the Experimental Section).

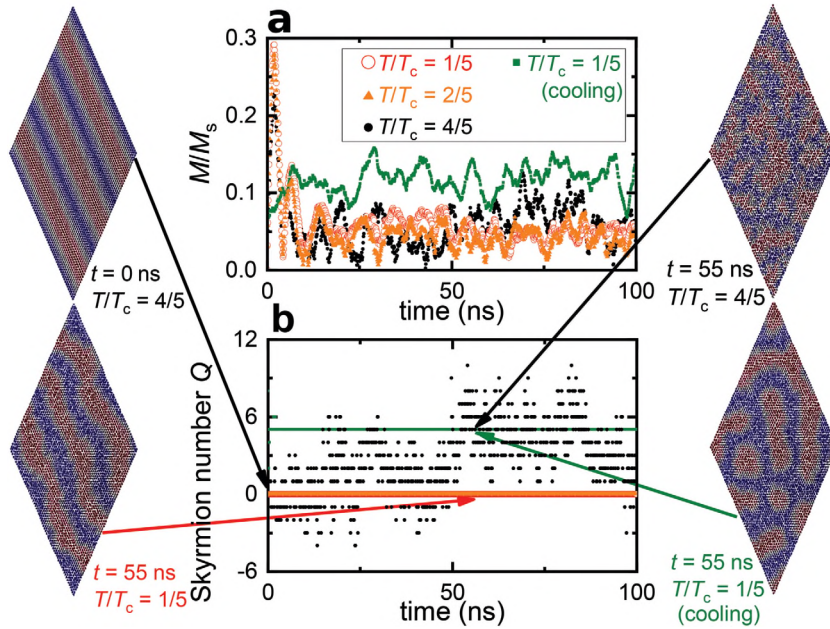


Figure 5. Atomistic simulations of the thermal skyrmion creation. a) The magnetization M and b) the skyrmion number Q as a function of time for different substrate temperatures.

temperatures corresponding to 20%, 40%, and 80% of T_c , starting from the demagnetized stripes state. The spin texture then thermalizes within several nanoseconds in the presence of a small magnetic field, which results in the net magnetization increasing from $M/M_s = 0$ to ≈ 0.05 as shown in Figure 5a. At low temperature, the probability of creating isolated skyrmions is too low and therefore the skyrmion number Q (which can only take integer values) remains constant and zero as shown in Figure 5b. This probability, however, increases exponentially with temperature^[42] and raising T to $4/5T_c$ is enough to create and delete skyrmions every 0.1 ns (see the Video in the Supporting Information) as shown in the fluctuations of Q (black points). The average Q at this temperature still remains zero.

We then take the spin texture at $4/5T_c$ and cool it down to $1/5T_c$ (the applied current is switched off in experiments) as shown with the green points in Figure 5a,b. After cooling, the magnetization increases up to 0.1, which indicates the presence of skyrmions.^[43] Note that the resulting skyrmions remain frozen and with a finite Q . As a side note, since thermal excitations are achiral, both skyrmions and antiskyrmions can be created, but in our case, the DMI favors skyrmions over antiskyrmions, which results in a very short lifetime for the latter. Also, the entropic effects, which become relevant at temperatures approaching T_c ,^[44] are not accounted for by our analysis.

Since we have shown that thermal excitations can create skyrmions, we now demonstrate that one can controllably transition between stable and metastable states using fields and applied currents. We use as an example the generation and current-induced motion of skyrmions at room temperature and zero field, which, as shown before, are not the ground state under these conditions. We first generate a skyrmionic state (Figure 6a,b) from the labyrinth state at an OOP field of 20 mT (or likewise, from the demagnetized state as in Figure 6f-h),

which shifts the ground state configuration from stripes to a skyrmion lattice. The temperature rise enables the system to reach the new ground state, and after subsequently removing the field, the skyrmions indeed survive (Figure 6c,i). Their radius, though, increases in order to decrease the net magnetostatic energy. These zero-field skyrmions can subsequently be displaced by unipolar current pulses (Figure 6c,d) as long as the Joule heating is low enough to prevent recovery of the stripe-like ground state. This transition is evident after the application of bipolar pulse trains (Figure 6e,j), where the cumulative heating eventually changes the morphology of the system into the aligned stripes state.

We have seen that at room temperature, the skyrmionic state remains stable only under some bias magnetic field, $B > B_{\text{thr}}$ (Figures 6b,h). However, at higher temperatures we find that the point of the skyrmionic transition B_{thr} shifts to lower fields. This trend is illustrated in Figure 6k, where we plot the states that result from applying bipolar pulse trains of amplitude (U) as a function of the OOP field (B) and the substrate temperature (T). For voltages below 1.3 V, the initial labyrinth state remains unchanged, which, in line with our earlier discussion, is likely due to an insufficient thermal energy to overcome the morphological barriers. However, the B - T slice at $U = 2.6$ V represents a particular interest, as it reveals that: i) for temperatures above 350 K *stable* skyrmions can be found even at zero field, ii) our multilayers qualitatively follow the established trend in field-temperature bulk phase diagrams of the stripes-to-bubbles^[44-47] and stripes-to-skyrmions transitions.^[26,27] Our work, thus, constitutes the first experimental demonstration that a similar phase space exists in high-DMI and applications relevant metallic thin film systems at elevated temperatures.

In summary, we have shown that ultralow-pinning Pt/CoFeB/MgO multilayer stacks exhibit several distinct morphological phases whose stability is dictated by temperature and applied field. Transitions between phases can be triggered by transient Joule heating due to current-pulse injection which, in combination with the applied field, allows us to select desired phases and create magnetic skyrmions on demand. A valid technological implication of our results then is that by applying heating locally one could create skyrmions in predetermined areas in a device. These heat-induced skyrmions, unlike the ones generated by defects,^[22,31,32] could then be displaced freely without the need to drive them away from a pinning site. We demonstrate that in this material, an entire array of skyrmions can be generated reliably with just a single few-nanosecond-long pulse. Finally, we establish multiple ways to obtain the zero-field skyrmions that can be readily manipulated by current. Our findings provide new fundamental insights and reveal new mechanisms for the creation of skyrmions, which are essential ingredients for future spintronic applications.

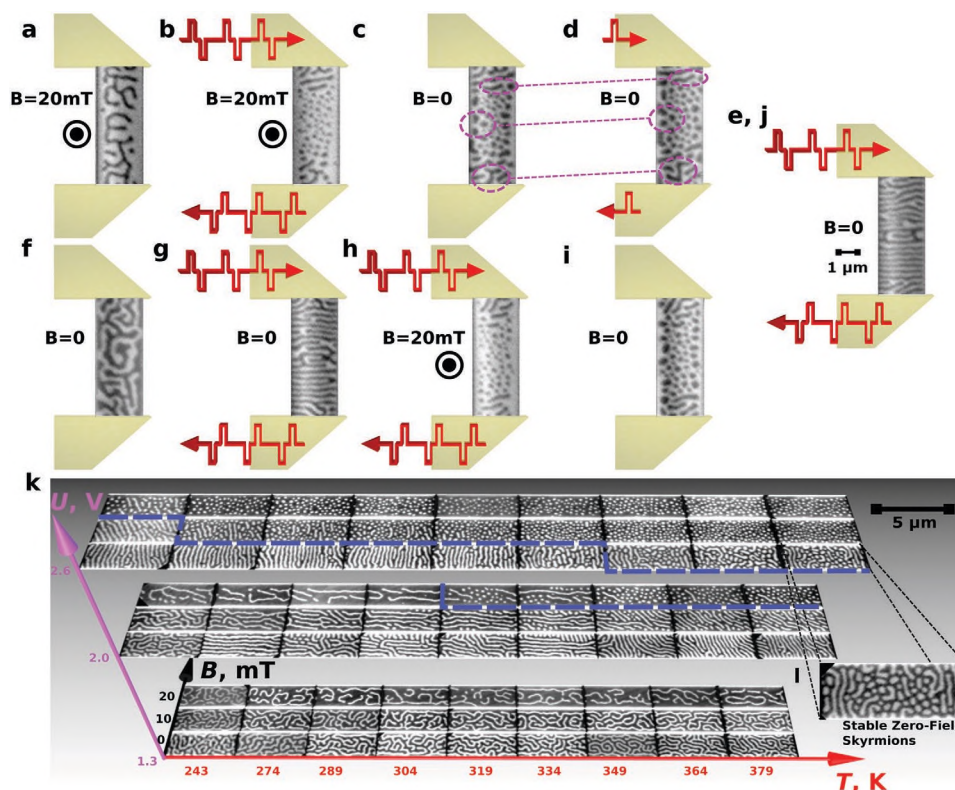


Figure 6. a–e) The generation of metastable zero field room-temperature skyrmions from a magnetized (stable) skyrmions state (b), which, in turn, has been directly obtained by applying 100 bipolar pulses of 2.7 V to a labyrinth state (a). c,d) Zero field metastable skyrmions achieved by removing the OOP field. c,d) The uniform motion of zero-field skyrmions after the application of three unipolar pulses of 2.7 V amplitude and 5 ns duration. e) The subsequent stable stripe state that was created from the application of bipolar pulses to such metastable skyrmions state. f–j) The generation of metastable zero field room-temperature skyrmions (i) from the stable skyrmion state (h), which in turn was obtained from a zero field stripe state (g). k) Experimental B – T – U phase diagram. Each state is obtained from the initial labyrinth state by injecting 10 000 bipolar pulse excitations with a period of 2 μ s and the distance between bipolar pulses of 1 μ s. Each individual pulse has a width of 7.5 ns with a sub-nanosecond rise time. Note that injecting stronger pulses is similar in effect to raising the substrate temperature. l) Stable zero field skyrmions (mixed with stripes) that were attained at the substrate temperature of 379 K by application of pulse trains directly to the 0 mT initial state.

Experimental Section

The details of the experimental and simulation methods are available in the Supporting Information.

Supporting Information

Supporting Information is available from the Wiley Online Library or from the author.

Acknowledgements

The author contributions are listed in the Supporting Information. This work was supported by the U.S. Department of Energy (DOE), Office of Science, Basic Energy Sciences (BES) under Award #DE-SC0012371. M.K. and the group at Mainz acknowledge support by the DFG (in particular SFB TRR173 Spin+X and SPP 2137 Skyrmionics), the Graduate School of Excellence Materials Science in Mainz (MAINZ, GSC 266), the EU (MultiRev (ERC-2014-PoC 665672), WALL (FP7-PEOPLE-2013-ITN 608031)), SpinNet, a topical network project of the German Academic Exchange Service (DAAD), and the Research Center of Innovative and Emerging Materials at Johannes Gutenberg University (CINEMA). K.L. and M.B. gratefully acknowledges financial support by the Graduate

School of Excellence Materials Science in Mainz (MAINZ). K.L. and N.K. gratefully acknowledge financial support of the German Academic Scholarship Foundation. F.B. acknowledges financial support by the German Research Foundation through grant no. BU 3297/1-1. The PolLux endstation was financed by the German Minister für Bildung und Forschung (BMBF) through contracts 05KS4WE1/6 and 05KS7WE1. M.-Y.I. acknowledges support by Leading Foreign Research Institute Recruitment and Future Materials Discovery Programs through the NRF of Korea (2018K1A4A3A03075584, 2016M3D1A1027831, 2017R1A4A1015323), the DGIST R&D program of the Ministry of Science, ICT and future Planning (18-BT-02), and by DOE-BES under contract #DE-AC02-05CH11231.

Conflict of Interest

The authors declare no conflict of interest.

Keywords

Dzyaloshinskii–Moriya interaction, magnetic domains, multilayers, perpendicular magnetic anisotropy, skyrmions

- [1] T. Jeong, W. E. Pickett, *Phys. Rev. B: Condens. Matter Mater. Phys.* **2004**, *70*.
- [2] S. Mühlbauer, B. Binz, F. Jonietz, C. Pfleiderer, A. Rosch, A. Neubauer, R. Georgii, P. Böni, *Science* **2009**, *323*, 915.
- [3] X. Z. Yu, Y. Onose, N. Kanazawa, J. H. Park, J. H. Han, Y. Matsui, N. Nagaosa, Y. Tokura, *Nature* **2010**, *465*, 901.
- [4] F. Büttner, C. Moutafis, M. Schneider, B. Krüger, C. M. Günther, J. Geilhufe, C. v. Korff Schmising, J. Mohanty, B. Pfau, S. Schaffert, A. Bisig, M. Foerster, T. Schulz, C. A. F. Vaz, J. H. Franken, H. J. M. Swagten, M. Kläui, S. Eisebitt, *Nat. Phys.* **2015**, *11*, 225.
- [5] S. Woo, K. Litzius, B. Krüger, M.-Y. Im, L. Caretta, K. Richter, M. Mann, A. Krone, R. M. Reeve, M. Weigand, P. Agrawal, I. Limesh, M.-A. Mawass, P. Fischer, M. Kläui, G. S. D. Beach, *Nat. Mater.* **2016**, *15*, 501.
- [6] C. Moreau-Luchaire, C. Moutafis, N. Reyren, J. Sampaio, C. A. F. Vaz, N. Van Horne, K. Bouzehouane, K. Garcia, C. Deranlot, P. Warnicke, P. Wohlhüter, J.-M. George, M. Weigand, J. Raabe, V. Cros, A. Fert, *Nat. Nanotechnol.* **2016**, *11*, 731.
- [7] O. Boulle, J. Vogel, H. Yang, S. Pizzini, D. de S. Chaves, A. Locatelli, T. O. Menteş, A. Sala, L. D. Buda-Prejbeanu, O. Klein, M. Belmeguenai, Y. Roussigné, A. Stashkevich, S. M. Chérif, L. Aballe, M. Foerster, M. Chshiev, S. Auffret, I. M. Miron, G. Gaudin, *Nat. Nanotechnol.* **2016**, *11*, 449.
- [8] B. Dupé, M. Hoffmann, C. Paillard, S. Heinze, *Nat. Commun.* **2014**, *5*, 4030.
- [9] N. Romming, A. Kubetzka, C. Hanneken, K. Von Bergmann, R. Wiesendanger, *Phys. Rev. Lett.* **2015**, *114*, 177203.
- [10] S. von Malottki, B. Dupé, P. F. Bessarab, A. Delin, S. Heinze, *Sci. Rep.* **2017**, *7*, 1, 12299.
- [11] M. Hervé, B. Dupé, R. Lopes, M. Böttcher, M. D. Martins, T. Balashov, L. Gerhard, J. Sinova, W. Wulfhchel, *Nat. Commun.* **2018**, *9*, 1, 1015.
- [12] W. Jiang, X. Zhang, G. Yu, W. Zhang, X. Wang, M. B. Jungfleisch, J. E. Pearson, X. Cheng, O. Heinonen, K. L. Wang, Y. Zhou, A. Hoffmann, S. G. E. te Velthuis, *Nat. Phys.* **2017**, *13*, 162.
- [13] K. Litzius, I. Limesh, B. Krüger, P. Bassirian, L. Caretta, K. Richter, F. Büttner, K. Sato, O. A. Tretiakov, J. Förster, R. M. Reeve, M. Weigand, I. Bykova, H. Stoll, G. Schütz, G. S. D. Beach, M. Kläui, *Nat. Phys.* **2016**, *13*, 170.
- [14] A. Fert, V. Cros, J. Sampaio, *Nat. Nanotechnol.* **2013**, *8*, 152.
- [15] X. Zhang, M. Ezawa, Y. Zhou, *Sci. Rep.* **2015**, *5*, 9400.
- [16] J. Zázvorka, F. Jakobs, D. Heinze, N. Keil, S. Kromin, S. Jaiswal, K. Litzius, G. Jakob, P. Virnau, D. Pinna, K. Everschor-Sitte, A. Donges, U. Nowak, M. Kläui, arXiv:1805.05924 **2018**.
- [17] G. Bourianoff, D. Pinna, M. Sitte, K. Everschor-Sitte, *AIP Adv.* **2018**, *8*, 055602.
- [18] I. Dzyaloshinsky, *J. Phys. Chem. Solids* **1958**, *4*, 241.
- [19] T. Moriya, *Phys. Rev.* **1960**, *120*, 91.
- [20] R. Tomasello, E. Martinez, R. Zivieri, L. Torres, M. Carpentieri, G. Finocchio, *Sci. Rep.* **2014**, *4*, 6784.
- [21] W. Legrand, D. Maccariello, N. Reyren, K. Garcia, C. Moutafis, C. Moreau-Luchaire, S. Collin, K. Bouzehouane, V. Cros, A. Fert, *Nano Lett.* **2017**, *17*, 2703.
- [22] F. Büttner, I. Limesh, M. Schneider, B. Pfau, C. M. Günther, P. Helsing, J. Geilhufe, L. Caretta, D. Engel, B. Krüger, J. Viefhaus, S. Eisebitt, G. S. D. Beach, *Nat. Nanotechnol.* **2017**, *12*, 1040–1044.
- [23] N. Romming, C. Hanneken, M. Menzel, J. E. Bickel, B. Wolter, K. von Bergmann, A. Kubetzka, R. Wiesendanger, *Science* **2013**, *341*, 636.
- [24] J. Sampaio, V. Cros, S. Rohart, A. Thiaville, A. Fert, *Nat. Nanotechnol.* **2013**, *8*, 839.
- [25] The state we refer to as a skyrmion lattice state often exhibits considerable disorder and might better be characterized as a disordered array. However, for simplicity we refer to such states as a skyrmion lattice and note that disorder is common in skyrmion lattices, particularly in low-pinning materials where it is known to have negligible impact on the total energy of the state.^[38]
- [26] S. Buhrandt, L. Fritz, *Phys. Rev. B* **2013**, *88*, 195137.
- [27] S. A. Montoya, S. Couture, J. J. Chess, J. C. T. Lee, N. Kent, D. Henze, S. K. Sinha, M.-Y. Im, S. D. Kevan, P. Fischer, B. J. McMorrin, V. Lomakin, S. Roy, E. E. Fullerton, *Phys. Rev. B* **2017**, *95*, 024415.
- [28] W. Jiang, P. Upadhyaya, W. Zhang, G. Yu, M. B. Jungfleisch, F. Y. Fradin, J. E. Pearson, Y. Tserkovnyak, K. L. Wang, O. Heinonen, S. G. E. te Velthuis, A. Hoffmann, *Science* **2015**, *349*, 283.
- [29] O. Heinonen, W. Jiang, H. Somaily, S. G. E. Te Velthuis, A. Hoffmann, *Phys. Rev. B* **2016**, *93*, 094407.
- [30] J. Müller, A. Rosch, *Phys. Rev. B* **2015**, *91*, 054410.
- [31] M. Sitte, K. Everschor-Sitte, T. Valet, D. R. Rodrigues, J. Sinova, A. Abanov, *Phys. Rev. B* **2016**, *94*, 064422.
- [32] K. Everschor-Sitte, M. Sitte, T. Valet, J. Sinova, A. Abanov, *New J. Phys.* **2017**, *19*, 092001.
- [33] W. Koshibae, N. Nagaosa, *Nat. Commun.* **2016**, *7*, 10542.
- [34] U. Ritzmann, S. von Malottki, J.-V. Kim, S. Heinze, J. Sinova, B. Dupé, *Nat. Electronics.* **2018**, *1*, 451.
- [35] M. Böttcher, S. Heinze, S. A. Egorov, J. Sinova, B. Dupé, *New J. Phys.* **2018**, <https://doi.org/10.1088/1367-2630/aae282>.
- [36] I. Limesh, F. Büttner, G. S. D. Beach, *Phys. Rev. B* **2017**, *95*, 174423.
- [37] J. A. Cape, G. W. Lehman, *J. Appl. Phys.* **1971**, *42*, 5732.
- [38] C. B. Muratov, *Phys. Rev. E: Stat., Nonlinear, Soft Matter Phys.* **2002**, *66*, 066108.
- [39] S. Emori, U. Bauer, S.-M. Ahn, E. Martinez, G. S. D. Beach, *Nat. Mater.* **2013**, *12*, 611.
- [40] J. Sinova, S. O. Valenzuela, J. Wunderlich, C. H. Back, T. Jungwirth, *Rev. Mod. Phys.* **2015**, *87*, 1213.
- [41] H. Fangohr, H. Fangohr, D. S. Chernyshenko, M. Franchin, T. Fischbacher, G. Meier, *Phys. Rev. B* **2011**, *84*, 054437.
- [42] S. Rohart, J. Miltat, A. Thiaville, *Phys. Rev. B* **2016**, *93*, 214412.
- [43] Skyrmions tend to cover less area due to a skyrmion–skyrmion repulsion.
- [44] E. A. Zavadskii, V. A. Zablotskii, *Phys. Status Solidi A* **1989**, *112*, 145.
- [45] T. Garel, S. Doniach, *Phys. Rev. B* **1982**, *26*, 325.
- [46] M. Seul, R. Wolfe, *Phys. Rev. A* **1992**, *46*, 7519.
- [47] M. Seul, D. Andelman, *Science* **1995**, *267*, 476.